http://pubs.acs.org/journal/aelccp

# Navigating *iR* Compensation: Practical Considerations for Accurate Study of Oxygen Evolution Catalytic Electrodes



Downloaded via UNIV OF TEXAS AT AUSTIN on December 5, 2023 at 22:47:06 (UTC). See https://pubs.acs.org/sharingguidelines for options on how to legitimately share published articles.

Cite This: ACS Energy Lett. 2023, 8, 4323–4329



**ACCESS** I

III Metrics & More

Article Recommendations

s Supporting Information

'n a three-electrode electrochemical system, uncompensated resistance  $(R_u)$  between the working and reference electrodes results in an electrostatic potential drop called iR potential drop, where i is a measured current. This iR potential drop skews the applied potential, meaning the potential set by the electrochemist is not the true applied potential. Thus, iR compensation needs to be performed to study the potential-dependent electrochemical behavior precisely. There are three commonly used methods for iR compensation: (1) positive feedback (PF), (2) current interrupt (CI), and (3) post-iR compensation after electrochemical analysis (Post).<sup>3,4</sup> For the R<sub>11</sub> measurement, alternating current (AC) technique-based electrochemical impedance spectroscopy (EIS) analysis, either automatically by software or manually, is used for PF and Post compensation methods. On the other hand, direct current (DC) techniquebased current interruption is used for the CI compensation method (see Supporting Note 1 for details about the  $R_n$ measurement and iR compensation methods).

However, despite the common use of the aforementioned compensation methods, there is a potential risk of performing inaccurate iR compensation that may lead to misleading results. This risk can arise from a lack of understanding of the underlying concepts and experimental and analytical methodologies involved in these compensation methods. Numerous studies and reviews have been conducted to address the concerns related to iR compensation. These studies focus on topics such as the identity of  $R_{\rm u}$  and  $i_{\rm v}^{5,6}$  measurement and selection of  $R_{\rm w}^{2,6}$  minimization of  $R_{\rm w}^2$  overcompensation of iR potential drop, ambiguity about the degree of iR compensation, inconsistent results from different iR compensation methods, and data processing for post iR compensation.

Nevertheless, the practical application of iR compensation, in terms of accurate measurement and interpretation of  $R_{\rm u}$ , selection of an appropriate iR compensation method, and understanding their effects on electrochemical analyses, as depicted in Figure 1, remains a challenging task. This is primarily due to the complexity of various electrochemical systems. Depending on factors such as the specific electrochemical reaction (e.g., water electrolysis and  $CO_2$  electrolysis), electrode properties (e.g., composition and structure), and experimental conditions for electrochemical testing (e.g., electrolyte, cell design, applied potential, and operating

current), the physical identity of  $R_{\rm u}$  and its compatibility with a particular iR compensation method can vary significantly.

The three-electrode alkaline oxygen evolution reaction (OER) system presents several unique characteristics that should be considered when applying iR compensation. First, alkaline OER electrocatalysts based on 3d-transition metals (e.g., Ni, Co, and Fe) commonly form hydrous metal (oxy)hydroxides  $(MO_xH_y)$  during the OER. 9-12 These MO<sub>x</sub>H<sub>v</sub> phases typically exhibit low electrical conductivity and become more conductive after the anodic redox reaction  $(M^{2+}/M^{3+})$ . In addition, the solution resistance, which conventionally represents  $R_{11}$ , remains constant and relatively small (around 2  $\Omega$ ) due to the highly ionic conductive electrolytes (e.g., 1 M KOH) and the short distance between the working and reference electrodes.2 Accordingly, the resistance on the working electrode side can become a relatively significant component of R<sub>u</sub> compared to other electrochemical systems with significant solution resistance (e.g., CO<sub>2</sub> reduction in 0.1 M KHCO<sub>3</sub>). Considering these factors,  $R_n$  in the alkaline OER system can consist of four main components, as illustrated in Figure 1a: (1) solution resistance, (2) gas bubble-induced solution resistance at the catalyst/ electrolyte interface ( $R_{\text{bubble}}$ ), (3) electron transport resistance through the electrode  $(R_{et})$ , and (4) contact impedance  $(Z_{contact})$  at the electrode holder/substrate or substrate/catalyst interface.  $^{5,6,13}$  Furthermore, the  $R_{\rm u}$  components originating from the working electrode ( $Z_{contact}$ ,  $R_{et}$ , and  $R_{bubble}$ ) can change dynamically depending on the electrode properties and electrochemical testing conditions. <sup>6,13</sup> Here, note that the  $R_{\rm u}$  of the electrode consisting of a porous or completely electrolytepermeable catalyst layer on the substrate does not include the  $R_{\rm et}$  through the catalyst layer, but only through the substrate.<sup>2,6,14</sup>

In this Viewpoint, we study the *iR* compensation for the alkaline OER system as a case study. We aim to identify the

Received: August 10, 2023 Accepted: September 12, 2023 Published: September 22, 2023





# (a) Components of $R_u$

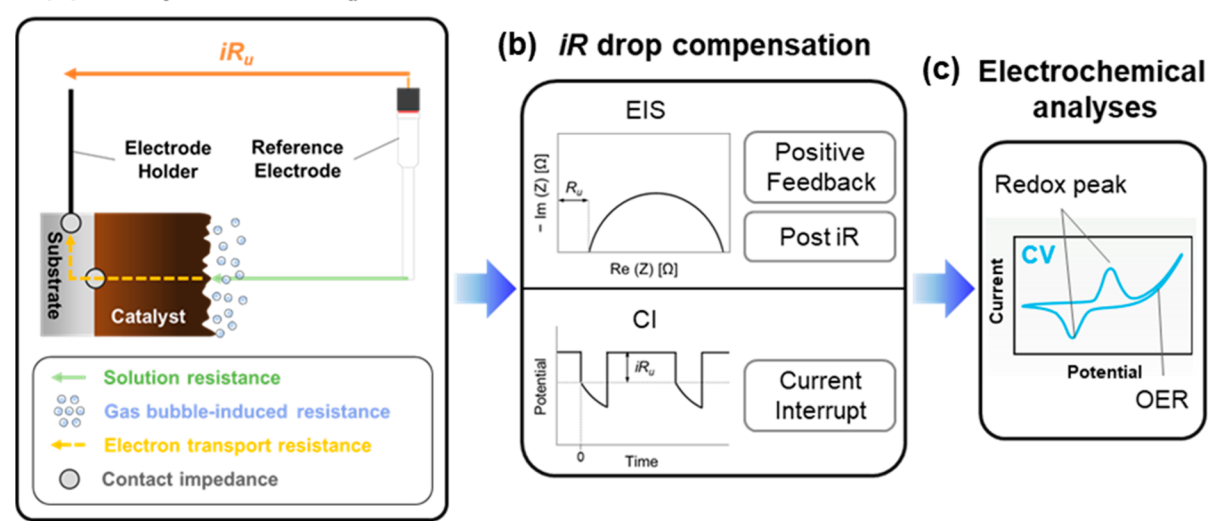


Figure 1. Schematic illustration depicting (a) the components of  $R_u$  in a three-electrode electrochemical system for a gas-evolving catalytic electrode, (b) methods used for  $R_u$  measurement and iR drop compensation, and (c) the reaction of interest for electrochemical analysis: either redox reaction of the electrode or electrocatalytic reaction (e.g., OER).

experimental pitfalls that can arise when applying iR compensation to the study of catalytic electrodes. First, we discuss several cases in which the same catalytic electrode exhibits different OER activity depending on the methods used for  $R_{ij}$  measurement and iR compensation. To understand the underlying causes behind this issue, we investigate the roles of different  $R_{ij}$  components in iR compensation depending on the electrode properties and electrochemical testing conditions. Furthermore, we demonstrate that the results obtained from potentiodynamic analysis of the electrode's redox reaction can vary depending on the method and degree of iR compensation. These variations are attributed to a change in the actual scan rate near the redox peak during potentiodynamic analysis and the occurrence of electron -rapping phenomena within the electrode. Lastly, we provide practical guidelines on how to correctly measure and interpret the  $R_{\rm u}$  value and how to select the proper iR compensation method for studying the redox reaction and electrocatalytic activity of the electrode.

**Inconsistent Electrocatalytic Activity Due to Incorrect** or Varying  $R_{u}$ . To investigate the influence of iRcompensation on electrochemical analyses of catalytic electrodes, we conducted experiments using Ni and Co-based catalyst films on conductive substrates, such as fluorine-doped tin oxide (FTO) glass, Ni foil, and Ni foam. Details of these prepared electrodes are summarized in Table S1. Moreover, different types of electrode holders (e.g., alligator clip, Ti clip, and Pt clip) were used to connect the electrodes to the potentiostat (Figure S1). Cyclic voltammetry (CV) tests using Ni-based electrodes with distinct properties (e.g., presence or absence of contact impedance, varying  $R_u$ , and redox peak distortion) were conducted in a 1 M KOH electrolyte (Figure 2a-d). The CV curves presented in each panel of Figure 2 were obtained from the same catalytic electrode but employing different methods and degrees of iR compensation. The abbreviation "CI" represents the current-interrupt method with 100% iR compensation. On the other hand, "PF 100%", "PF 85%", and "PF 70%" denote the positive feedback method with iR compensation degrees of 100%, 85%, and 70%, respectively.

Additionally, "No iR" indicates the absence of iR compensation.

The formation of an insulating oxide layer on either the electrode holders or substrates can lead to poor contact at the electrode holder/substrate interface, resulting in the development of contact impedance. In Figure 2a, CV curves of the NiO<sub>x</sub>H<sub>y</sub>/FTO electrode connected with an alligator clip highlight a potential problem for iR compensation caused by the contact impedance at the electrode holder/substrate interface. Interestingly, despite both the CI and PF 100% utilizing full iR compensation, different OER activities were obtained; CI exhibits higher OER activity than PF 100%. Additionally, when comparing CI with PF 100%, noticeable differences in the shape and peak current density of the redox peaks corresponding to the Ni<sup>2+/3+</sup> anodic redox reaction at approximately 1.36 V were observed, which will be further discussed in a later section. To gain insight into the observed differences in OER activity, the  $R_u$  values employed for iR compensation during the CV were examined by analyzing the slope of the uncompensated potential drop  $(V_{ij})$  versus current density (j), as shown in Figure S2. The  $R_u$  value employed for CI  $(R_{u,CI})$  was 7.51  $\Omega$  cm<sup>2</sup>, which is higher than the 6.83  $\Omega$ cm<sup>2</sup> value for PF 100%. These results demonstrate that different R<sub>u</sub> values modified the iR compensation and influenced the measured OER activity.

The discrepancy in  $R_{\rm u}$  values between PF and CI arises from the fact that  $R_{\rm u}$  measurement methods, which are EIS (either automatic or manual) and current interruption for PF and CI, respectively, are affected by the contact impedance at the electrode holder/substrate interface differently. The contact impedance can be detected through EIS, appearing as a semicircle on the Nyquist plot or a peak in the Bode phase plot in the high-frequency region  $(10^4-10^5\ Hz)$ , in addition to those related to faradaic reactions (e.g., OER or redox reaction of the electrode) in the low-frequency region (Figures S3 and S4). Note that the contact impedance is challenging to detect at nonfaradaic potentials (e.g., open-circuit potential) or potentials where fast faradaic reactions (e.g., Ni<sup>2+/3+</sup> redox reaction) occur, but it becomes evident at potentials where

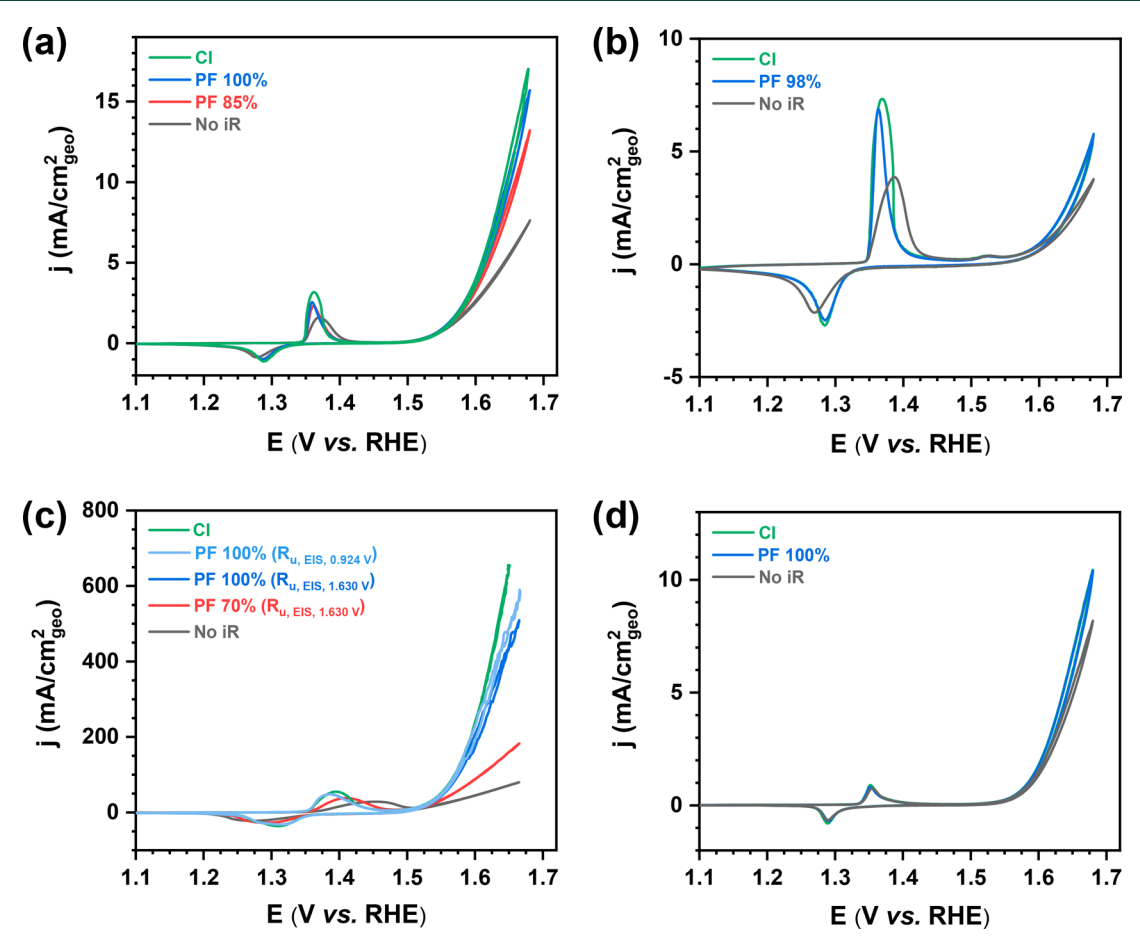


Figure 2. CV curves of Ni-based electrodes in 1 M KOH electrolyte at a scan rate of 10 mV/s employing different methods and degrees of iR compensation. (a) NiO<sub>x</sub>H<sub>y</sub>/FTO: contact impedance, constant  $R_{\rm uv}$  and redox peak distortion for CI; (b) NiO<sub>x</sub>H<sub>y</sub>/FTO: no contact impedance, constant  $R_{\rm uv}$  and redox peak distortion for CI; (c) nanoporous NiO<sub>x</sub>H<sub>y</sub>/Ni foam: no contact impedance, varying  $R_{\rm uv}$  and redox peak distortion for CI; and (d) Ni foil: no contact impedance, constant  $R_{\rm uv}$ , and no redox peak distortion for CI.

slow faradaic reactions (e.g., OER) occur. Further details about the contact impedance at the electrode holder/substrate interface, including its experimental identification, origin, how to avoid it, equivalent circuit representation, and different shapes, can be found in the Supporting Notes 2.1–2.4 and Figures S3–S18. As shown in Figure S11, manual EIS analysis conducted at appropriate potentials can not only measure  $R_{\rm u}$  correctly but also provide two different  $R_{\rm u}$  values by distinguishing the contact impedance:  $R_{\rm u,EIS,1}$  (6.83  $\Omega$  cm²) at 268.4 kHz, excluding the contact impedance, and  $R_{\rm u,EIS,2}$  (7.69  $\Omega$  cm²) at 2.659 kHz, including the contact impedance. Moreover, the  $R_{\rm u}$  value measured from the automatic EIS ( $R_{\rm u,auto}$ ) for PF 100% in Figure S2 was equivalent to the  $R_{\rm u,EIS,1}$  (see Supporting Note 2.5 for cautions about EIS-based  $R_{\rm u}$  measurement in the presence of contact impedance).

The DC technique-based current interruption method is typically used to measure the series resistance in an electrochemical system, which corresponds to the  $R_{\rm u,EIS,1}$  from EIS analysis. However, we observed that  $R_{\rm u,CI}$  (7.51  $\Omega$  cm²) was overestimated compared to  $R_{\rm u,EIS,1}$  (6.83  $\Omega$  cm²). This overestimation of  $R_{\rm u,CI}$  can be attributed to the presence of a small contact capacitance at the electrode holder/substrate interface, resulting in a small RC time constant for the contact impedance, which is not sufficiently large compared to the current interruption sampling time ( $t_{\rm sampling}$ ) (see Supporting Note 2.6, Figure S19, and Table S2 for a detailed explanation

regarding the failure of CI in the presence of contact impedance at the electrode holder/substrate interface). Therefore, we recommend exercising caution when employing the CI method in the presence of contact impedance to ensure accurate *iR* compensation.

Figure 2b shows the CV curves of the NiO<sub>x</sub>H<sub>v</sub>/FTO electrode without contact impedance at the electrode holder/ substrate interface. The electrode was connected with a new/ polished alligator clip to ensure good contact at the electrode holder/substrate interface. The CI and PF 98% exhibited almost identical OER activity, and their corresponding  $R_{11}$ values were almost identical:  $R_{u,CI}$  (6.06  $\Omega$  cm<sup>2</sup>) and  $R_{u,EIS}$  $(6.10 \ \Omega \ cm^2)$  (Figures S20 and S21). This result indicates that the CI method evaluates the OER activity accurately in the absence of contact impedance (Figure S21). Additionally, similar to the case of the NiO, H,/FTO electrode with contact impedance (Figure 2a), the differences in the shape and peak current density for Ni<sup>2+/3+</sup> redox reaction peaks were observed in Figure 2b, implying that the contact impedance is not responsible for the observed redox peak difference between CI and PF. However, we noticed the formation of contact impedance after OER testing (Figure S22). This newly developed contact impedance may originate from the substrate/catalyst layer interface, caused by poor adhesion of the NiO, H, catalyst layer to the FTO substrate after the OER testing. On the other hand, the self-supported electrode (NiCV), which possesses better adhesion between the catalyst layer and the substrate, did not develop contact impedance even after the OER testing (see Supporting Note 2.7 and Figures \$23–\$25).

The contact impedance at the substrate/catalyst interface and its impact on iR compensation was further explored by investigating the NiO<sub>x</sub>H<sub>y</sub>/Ni foil electrode before and after peeling off the NiO<sub>x</sub>H<sub>v</sub> catalyst layer from the Ni foil substrate (see Supporting Note 2.7 and Figures S26 and S27). However, unlike the contact impedance at the electrode holder/substrate interface, the contact impedance at the substrate/catalyst interface did not cause an overestimation of R<sub>u,CI</sub> compared to  $R_{\text{n,FIS}}$  (Figure S28). This is due to the sufficiently large capacitance and RC time constant at the substrate/catalyst interface, in contrast to the small capacitance and RC time constant at the electrode holder/substrate interface (see Supporting Note 2.7 and Table S3). In summary, contact impedance can occur at both the electrode holder/substrate interface and the substrate/catalyst interface, before and after the OER testing. The contact impedance can result in two different  $R_u$  values, namely  $R_{u,EIS,1}$  and  $R_{u,EIS,2}$  (Figures S11, S13, S16, and S22). Moreover, depending on its unique characteristics (i.e., RC time constant relative to  $t_{\text{sampling}}$ ), the contact impedance can lead to either inaccurate or accurate iR compensation when using the CI method.

Certain components of  $R_u$  from the working electrode, such as  $R_{\rm et}$  and  $R_{\rm bubble}$ , can vary with the applied potential and operating current during OER testing. The CV curves in Figure 2c of the nanoporous NiO<sub>x</sub>H<sub>v</sub>/Ni foam electrode, which has a large surface area and high operating current density, demonstrate the effect of varying R<sub>u</sub> on iR compensation and the measured OER activity. When applying PF 100% with R<sub>u,EIS</sub> values measured at different potentials (0.924 and 1.630 V, which are below and above the Ni<sup>2+/3+</sup> anodic redox reaction potential, respectively), PF 100%  $(R_{u,EIS,0.924V})$  exhibited higher activity compared to PF 100%  $(R_{u, EIS, 1.630V})$ . This difference in activity was attributed to the smaller  $R_{\rm u,EIS 1.630V}$  (1.40  $\Omega$  cm<sup>2</sup>) compared to  $R_{\rm u,EIS 1.630V}$ (1.423  $\Omega$  cm<sup>2</sup>), as indicated by the EIS Nyquist plots in Figure S29b,c. This discrepancy in  $R_{u,EIS}$  values occurs due to the change in  $R_{\rm et}$  of the catalyst layer, which becomes detectable for sufficiently thick catalyst layers. Specifically, the electrical conductivity enhancement of NiOOH (Ni3+) at 1.630 V leads to a decrease in  $R_{\rm et}$  compared to the insulating Ni(OH)<sub>2</sub> (Ni<sup>2+</sup>) at 0.924 V.<sup>15,16</sup> (see Supporting Note 3.1 for details about the electrode properties of the Nanoporous  $NiO_xH_y/Ni$  foam related to the  $R_{et}$  measurement).

Moreover, despite the absence of contact impedance (as shown in Figure S29b,c), CI exhibited significantly higher OER activity (655 mA/cm<sup>2</sup>) compared to PF 100% (438.7 mA/ cm<sup>2</sup>) at 1.65 V. The higher OER activity of CI compared to PF 100% ( $R_{u,EIS,1.630V}$ ) is attributed to the higher  $R_{u,CI}$  at OER potentials compared to  $R_{\rm u,EIS,1.630V}$ . The plots of  $V_{\rm u}$  versus j in Figure S30 show the variation of  $R_{u,CI}$  depending on the current density region. R<sub>u,CI</sub> at potentials below the OER onset potential was 1.40  $\Omega$  cm<sup>2</sup>, which is the same as  $R_{u,EIS,1.630V}$ . However, as the OER current density increased,  $R_{u,CI}$  increased to 1.45 and 1.49  $\Omega$  cm<sup>2</sup> due to the accumulation of oxygen bubbles (R<sub>bubble</sub>) during the OER. Here, it is noted that potential-dependent EIS analysis can detect the variation in  $R_{\rm et}$ but not the varying R<sub>bubble</sub>. On the other hand, the current interruption can detect the varying R<sub>bubble</sub>, but not the varying  $R_{\rm et}$ , although  $R_{\rm u,CI}$  reflects the  $R_{\rm et}$  of the MOOH active phase

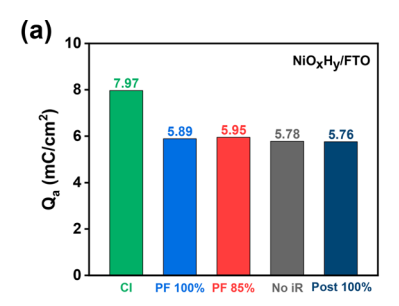
instead of the  $R_{\rm et}$  of M(OH)<sub>2</sub> (see Supporting Note 3.2 for details about characteristics and limitations of EIS and current interruption for measuring the varying  $R_{\rm u}$ ). The above results indicate that even slight differences in  $R_{\rm u}$  values, such as 0.023  $\Omega$  cm² due to varying  $R_{\rm et}$  and 0.09  $\Omega$  cm² due to varying  $R_{\rm bubble}$ , can lead to significant differences in OER activity at high operating current densities. Therefore, it is crucial to exercise caution and choose the proper method and condition for  $R_{\rm u}$  measurement and iR compensation (such as EIS at a specific applied potential or CI at a specific operating current density) based on the specific purpose of evaluating electrocatalytic performance (whether to include  $R_{\rm et}$  or  $R_{\rm bubble}$  in  $R_{\rm u}$  for iR compensation), especially for catalytic electrodes with large surface area and high operating current density.

Additionally, we examined a Ni foil electrode, which consists of a thin  $\mathrm{NiO_xH_y}$  catalyst layer on the surface of a Ni foil substrate and does not exhibit any contact impedance. This electrode was used as a control sample without any issues with the iR compensation method. In this case, CI and PF 100% showed identical OER activity,  $R_\mathrm{u}$  value, and shape and current density of the redox peak (Figure 2d and Figure S31). Furthermore, the  $R_\mathrm{u}$  variation by potential-dependent  $R_\mathrm{et}$  or current density-dependent  $R_\mathrm{bubble}$  was not observed in the Ni foil electrode. This lack of  $R_\mathrm{u}$  variation can be due to the thin thickness of the  $\mathrm{NiO_xH_y}$  catalyst layer, which possesses good electron transport properties, and the low operating current density, which does not lead to severe bubble accumulation near the electrode.

**Inaccurate Redox Peak Analysis Due to Scan Rate Variation and Electron Trapping.** The analysis of redox peaks for the electrode's redox reaction provides critical information about electrode properties, such as composition and crystal phase of the catalyst layer, variations in the coverage of reaction intermediate with applied potential, electrochemical reversibility of the redox reaction, whether the redox reaction is surface reaction-controlled or diffusion-controlled, and the number of electrochemically active redox sites. 9,15,17–19 Therefore, it is important to investigate the potential impact of *iR* compensation on the redox peak analysis to understand the aforementioned electrode properties accurately. Unfortunately, these considerations have often been overlooked in previous studies on *iR* compensation.

As demonstrated in Figure 2 and Figure S12, the shape and peak current density of redox peaks can be influenced by the degree of iR compensation and post-iR compensation method employed. However, the redox charge, which often serves as an indicator of the electrochemically active surface area of the catalytic electrode, 9,20 is expected to remain consistent regardless of the degree and method of iR compensation. Figure 3a and Figure S32 compare the redox charge for the  $Ni^{2+/3+}$  anodic redox reaction  $(Q_a)$  of the  $NiO_xH_y/FTO$ electrode in Figure 2a when different methods and degrees of iR compensation are employed. The  $Q_a$  values for PF 100%, PF 85%, No iR, and Post 100% were nearly identical, as expected, despite the different shapes and peak current densities of their redox peaks. On the other hand, the Q value for CI (7.97 mC/cm<sup>2</sup>) was 1.36 times higher than that of the other iR compensation methods. Moreover, CI exhibited a distinct redox peak shape and higher peak current density compared to PF 100% despite both methods utilizing the same 100% iR compensation.

The distinct redox peak properties of CI compared to PF 100% can be attributed to the variation in the actual scan rate



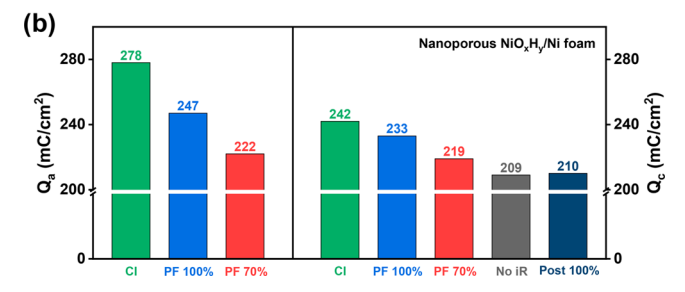


Figure 3. Electrochemical analysis of redox charge when employing different methods and degrees of iR compensation. (a)  $Q_a$  of the NiO<sub>x</sub>H<sub>y</sub>/FTO electrode in Figure 2a and (b)  $Q_a$  and  $Q_c$  of the nanoporous NiO<sub>x</sub>H<sub>y</sub>/Ni foam electrode in Figure 2c.

during the potentiodynamic analysis (e.g., CV) relative to the set scan rate. Figure S33 displays the plot of applied potential versus time during the CV analysis, where the slope represents the actual scan rate. While PF and No iR exhibited a constant slope of 10 mV/s, matching the set scan rate, CI showed a variation in the actual scan rate near the redox peak, which can change or even distort the shape of the redox peak. Furthermore, the actual scan rate of CI increased up to a maximum of 19.1 mV/s (Figure S33b), which can result in a higher redox peak current density  $(j_p)$  according to the relationship,  $j_p \propto (\text{scan rate})^b$ , where  $0.5 \le b \le 1.9,19$  The effect of the varying actual scan rates on the redox peak analysis was confirmed by comparing the anodic  $j_{\rm p}$  ( $j_{\rm pa}$ ) of CI measured at a set scan rate of 10 mV/s with  $j_{\rm pa}$  of PF 85% at 20 mV/s. Figure S34 demonstrates that CI (10 mV/s) and PF 85% (20 mV/s) exhibited identical redox peak current density due to their similar actual scan rates of approximately 20 mV/s. Therefore, it can be concluded that the distinct redox peak properties of CI, such as a different redox peak shape, overestimated  $j_p$  and  $Q_a$ , as well as a higher b-value in Figure S36, are a result of the variation in the actual scan rate near the redox peak, which was also observed in a previous report.

To investigate the origin of the variation in the actual scan rate for CI, control experiments were performed by changing the set scan rate and employing other OER catalysts with different electrical conductivity, such as CoO<sub>x</sub>H<sub>v</sub>, and NiCoO<sub>x</sub>H<sub>v</sub>. The results revealed that the variation in the actual scan rate for CI becomes more pronounced for more insulating materials and at higher scan rates (see Supporting Note 4.1, Figures S35-S39, and Table S4 for details). Based on the results of the control experiments and the working principle of CI, the variation in actual scan rate is likely caused by the fluctuation of the uncompensated voltage  $(V_n)$  near the redox peak during current interruption (Figures S37b,d, S38c,f, and S39c,f). This  $V_{\rm u}$  fluctuation can occur due to the in situ variation of the capacitance of the catalyst layer before and after the  $M^{2+/3+}$  redox reaction, which is caused by the difference in electrical conductivity between M(OH)<sub>2</sub> and

MOOH (see Supporting Note 4.2 and Figures S37–S39 for a detailed discussion). Hence, we note that OER catalysts, which are basically oxide-based materials with poor conductivity and conductivity-switching properties during the redox reaction, can potentially encounter the issue of redox peak distortion caused by the varying actual scan rate when using CI for potentiodynamic analysis.

Furthermore, we investigated the impact of *iR* compensation on the redox charge of practical OER catalytic electrodes with large surface area (i.e., high redox charge). In Figure 2c, different methods and degrees of iR compensation were employed for the Nanoporous NiO<sub>x</sub>H<sub>v</sub>/Ni foam electrode, and the resulting  $Q_{\rm a}$  and cathodic redox charge for  ${\rm Ni}^{2+/3+}$  redox reaction  $(Q_c)$  values were calculated and compared in Figures S40-S42 and Figure 3b. CI exhibited higher Q values compared to PF 100%, which can be due to the actual scan rate variation for CI, as shown in Figure S43. Unexpectedly, however, PF 100%, PF 70%, No iR, and Post 100% yielded different Q values, in contrast to the identical  $Q_a$  values observed for the NiO<sub>x</sub>H<sub>v</sub>/FTO electrode. A trend was observed where the Q value decreased when using a lower degree of iR compensation during the CV analysis: PF 100% > PF 70% > No  $iR \approx \text{Post } 100\%$ .

According to a previous report, catalytic electrodes with poor electron transport through thick catalyst layers may experience an electron trapping phenomenon, where portions of the redox active sites exposed to the electrolyte are not effectively utilized. This electron trapping phenomenon can occur in the Nanoporous  $\mathrm{NiO}_x\mathrm{H}_y/\mathrm{Ni}$  foam electrode due to its large surface area and thick catalyst layer, decreasing the measurable redox charge during the CV analysis. Our results suggest that a higher degree of iR compensation alleviates the electron trapping phenomenon, resulting in greater utilization of the redox active sites and consequently increasing the measurable amount of redox charge. This finding highlights the influence of the degree of iR compensation on the measurable amount of redox charge, particularly for catalytic electrodes with large surface areas and high redox charge.

Summary and Recommendations. While applying iR compensation may seem simple, our investigation reveals that its correct implementation in real experiments can be more complex and challenging than initially anticipated. In this Viewpoint, we demonstrate that the electrocatalytic activity and redox peak properties of OER catalytic electrodes can vary depending on the methods and conditions used for  $R_n$ measurement, as well as the type and degree of iR compensation employed. The potential pitfalls of iR compensation can occur due to the unique characteristics of the electrochemical system under investigation, which distinctly influence each  $R_{ii}$  measurement and iR compensation method. Thus, to ensure the proper application of  $R_n$ measurement and iR compensation as well as accurate interpretation of iR-compensated electrochemical data, we propose a recommended procedure along with critical factors to consider, which are outlined in Figure 4.

First, it is crucial to understand how each  $R_{\rm u}$  measurement method is affected by the electrode properties and electrochemical testing conditions for the correct measurement and interpretation of  $R_{\rm u}$ . This understanding will help distinguish the distinct roles of  $R_{\rm u}$  components (e.g.,  $Z_{\rm contact}$ ,  $R_{\rm et}$  and  $R_{\rm bubble}$ ) in the measured  $R_{\rm u}$  value (see Supporting Note 5 for more details). Next, when selecting the appropriate type and degree of iR compensation, it is critical to assess whether

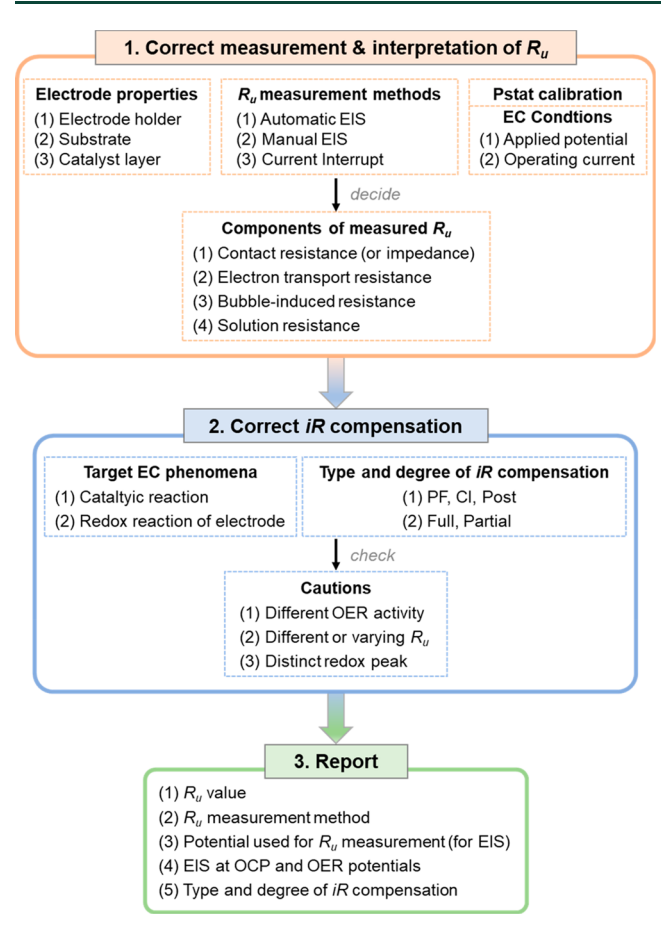


Figure 4. Recommended procedure and critical factors to consider for practical iR compensation for the study of OER catalytic electrodes.

variations in electrocatalytic activity, R<sub>u</sub> values, or redox peak properties are observed depending on the specific type and degree of iR compensation employed. Finally, it is essential to report comprehensive details regarding  $R_{ij}$  measurement and iRcompensation, including iR compensation and R<sub>11</sub> measurement methods, electrochemical conditions, such as the applied potential for EIS and the operating current during current interruption, as well as the  $R_{\rm u}$  value used for iR compensation. Additionally, regardless of the  $R_{\rm u}$  measurement and iRcompensation methods used, performing and reporting the potential-dependent EIS analyses are recommended to determine the presence of contact impedance or potentialdependent  $R_{\rm et}$  variations in the electrochemical system. In Supporting Note 6, we present specific recommendations and cautions related to iR compensation based on our data-driven findings. These recommendations cover the appropriate  $R_{ij}$ degree of iR compensation, and iR compensation method.

This Viewpoint provides essential electrochemical methodologies to interpret the meaning of the measured  $R_{ij}$  value and assess the suitability of the iR compensation method chosen. These methodologies include potential-dependent EIS, (scanrate dependent) CV, and data analysis techniques for determining the actual scan rate (from the slope of applied potential versus time) and  $R_{\rm u}$  (from the slope of  $V_{\rm u}$  versus j) during CV analysis. These methodologies for iR compensation enable direct evaluation of the catalytic electrode without additional control sample preparation, which can enhance the practicality of the iR compensation process. Furthermore, our

investigation provides potential explanations for issues observed in previous studies utilizing the CI method, such as a higher  $R_{\rm u,CI}$  value compared to  $R_{\rm u,EIS}$  despite the absence of *in situ* variation in solution resistance, <sup>21,22</sup> or the distortion of redox peak shapes during CV analysis. <sup>23</sup> The insights and methodologies for iR compensation presented in this Viewpoint are broadly applicable to the study of electrodes in electrochemical energy technologies, including electrocatalysis, batteries, and supercapacitors.

Yoon Jun Son orcid.org/0000-0003-1704-2314 Raul A. Marquez o orcid.org/0000-0003-3885-5007 Kenta Kawashima o orcid.org/0000-0001-7318-6115 Lettie A. Smith o orcid.org/0000-0003-0378-072X Chikaodili E. Chukwuneke orcid.org/0000-0003-0478-8387 Jerome Babauta

C. Buddie Mullins o orcid.org/0000-0003-1030-4801

#### ASSOCIATED CONTENT

#### Supporting Information

The Supporting Information is available free of charge at https://pubs.acs.org/doi/10.1021/acsenergylett.3c01658.

Full description of the experimental methods; Supporting Notes 1-6 (characteristics of R<sub>u</sub> measurement and iR compensation methods, contact impedance, varying  $R_{\rm u}$ , redox peak distortion, influence of electrochemical system on R<sub>11</sub> measurement, and recommendations and cautions about iR compensation); Figures S1-S43 (CV analyses with different scan rates or different types and degrees of iR compensation, charge integration and bvalue analyses for the redox peaks, estimation of actual scan rate and  $R_{\rm u}$  from the  $V_{\rm u}$  versus j plot using Gamry Echem Analysis software, EIS Nyquist and Bode phase plots at different potentials, and equivalent circuits for EIS fitting); and Tables S1-S4 (list of experimental samples, electrochemical parameters obtained from EIS fitting, and variation of actual scan rate with set scan rate for CI) (PDF)

### **AUTHOR INFORMATION**

Complete contact information is available at: https://pubs.acs.org/10.1021/acsenergylett.3c01658

#### Notes

Views expressed in this Viewpoint are those of the authors and not necessarily the views of the ACS.

The authors declare no competing financial interest.

#### ACKNOWLEDGMENTS

We gratefully acknowledge the National Science Foundation via Grant No. CHE-2102307 and the Robert A. Welch Foundation for their generous support through Grant No. F-1436.

## REFERENCES

(1) Bard, A. J.; Faulkner, L. R. Electrochemical Methods: Fundamentals and Applications, 2nd ed.; John Wiley & Sons, Inc.: New York, 2001. (2) Stevens, M. B.; Enman, L. J.; Batchellor, A. S.; Cosby, M. R.; Vise, A. E.; Trang, C. D. M.; Boettcher, S. W. Measurement Techniques for the Study of Thin Film Heterogeneous Water Oxidation Electrocatalysts. Chem. Mater. 2017, 29 (1), 120–140.

- (3) Oelßner, W.; Berthold, F.; Guth, U. The IR Drop Well-Known but Often Underestimated in Electrochemical Polarization Measurements and Corrosion Testing. *Mater. Corros.* **2006**, *57* (6), 455–466.
- (4) Heenan, A. R.; Hamonnet, J.; Marshall, A. T. Why Careful IR Compensation and Reporting of Electrode Potentials Are Critical for the CO2 Reduction Reaction. ACS Energy Lett. 2022, 7 (7), 2357–2361.
- (5) Britz, D. IR Elimination in Electrochemical Cells. *J. Electroanal. Chem. Interfacial Electrochem.* **1978**, 88 (3), 309–352.
- (6) Zheng, W. IR Compensation for Electrocatalysis Studies: Considerations and Recommendations. ACS Energy Lett. 2023, 8 (4), 1952–1958.
- (7) Anantharaj, S.; Noda, S. IR Drop Correction in Electrocatalysis: Everything One Needs to Know! *J. Mater. Chem. A* **2022**, *10* (17), 9348–9354.
- (8) Anantharaj, S.; Ede, S. R.; Karthick, K.; Sankar, S. S.; Sangeetha, K.; Karthik, P. E.; Kundu, S. Precision and Correctness in the Evaluation of Electrocatalytic Water Splitting: Revisiting Activity Parameters with a Critical Assessment. *Energy Environ. Sci.* **2018**, *11* (4), 744–771.
- (9) Son, Y. J.; Kim, S.; Leung, V.; Kawashima, K.; Noh, J.; Kim, K.; Marquez, R. A.; Carrasco-Jaim, O. A.; Smith, L. A.; Celio, H.; Milliron, D. J.; Korgel, B. A.; Mullins, C. B. Effects of Electrochemical Conditioning on Nickel-Based Oxygen Evolution Electrocatalysts. *ACS Catal.* **2022**, *12* (16), 10384–10399.
- (10) Son, Y. J.; Kawashima, K.; Márquez, R. A.; Smith, L. A.; Chukwuneke, C. E.; Mullins, C. B. Key Concepts for Understanding Alkaline Oxygen Evolution Reaction at the Atomic/Molecular Scale. *Curr. Opin. Electrochem.* **2023**, *39*, No. 101298.
- (11) Wygant, B. R.; Kawashima, K.; Mullins, C. B. Catalyst or Precatalyst? The Effect of Oxidation on Transition Metal Carbide, Pnictide, and Chalcogenide Oxygen Evolution Catalysts. *ACS Energy Lett.* **2018**, 3 (12), 2956–2966.
- (12) Kawashima, K.; Márquez-Montes, R. A.; Li, H.; Shin, K.; Cao, C. L.; Vo, K. M.; Son, Y. J.; Wygant, B. R.; Chunangad, A.; Youn, D. H.; Henkelman, G.; Ramos-Sánchez, V. H.; Mullins, C. B. Electrochemical Behavior of a Ni3N OER Precatalyst in Fe-Purified Alkaline Media: The Impact of Self-Oxidation and Fe Incorporation. *Mater. Adv.* 2021, 2 (7), 2299–2309.
- (13) Yu, L.; Ren, Z. Systematic Study of the Influence of IR Compensation on Water Electrolysis. *Mater. Today Phys.* **2020**, *14*, No. 100253.
- (14) Chung, D. Y.; Park, S.; Lopes, P. P.; Stamenkovic, V. R.; Sung, Y.-E.; Markovic, N. M.; Strmcnik, D. Electrokinetic Analysis of Poorly Conductive Electrocatalytic Materials. *ACS Catal.* **2020**, *10* (9), 4990–4996.
- (15) Trotochaud, L.; Young, S. L.; Ranney, J. K.; Boettcher, S. W. Nickel–Iron Oxyhydroxide Oxygen-Evolution Electrocatalysts: The Role of Intentional and Incidental Iron Incorporation. *J. Am. Chem. Soc.* **2014**, *136* (18), 6744–6753.
- (16) Batchellor, A. S.; Boettcher, S. W. Pulse-Electrodeposited Ni–Fe (Oxy)Hydroxide Oxygen Evolution Electrocatalysts with High Geometric and Intrinsic Activities at Large Mass Loadings. *ACS Catal.* **2015**, *5* (11), 6680–6689.
- (17) Klaus, S.; Cai, Y.; Louie, M. W.; Trotochaud, L.; Bell, A. T. Effects of Fe Electrolyte Impurities on Ni(OH)2/NiOOH Structure and Oxygen Evolution Activity. *J. Phys. Chem. C* **2015**, *119* (13), 7243–7254.
- (18) Son, Y. J.; Kawashima, K.; Wygant, B. R.; Lam, C. H.; Burrow, J. N.; Celio, H.; Dolocan, A.; Ekerdt, J. G.; Mullins, C. B. Anodized Nickel Foam for Oxygen Evolution Reaction in Fe-Free and Unpurified Alkaline Electrolytes at High Current Densities. *ACS Nano* **2021**, *15* (2), 3468–3480.
- (19) Fleischmann, S.; Mitchell, J. B.; Wang, R.; Zhan, C.; Jiang, D.; Presser, V.; Augustyn, V. Pseudocapacitance: From Fundamental Understanding to High Power Energy Storage Materials. *Chem. Rev.* **2020**, *120* (14), *6738*–*6782*.
- (20) Wei, C.; Sun, S.; Mandler, D.; Wang, X.; Qiao, S. Z.; Xu, Z. J. Approaches for Measuring the Surface Areas of Metal Oxide

- Electrocatalysts for Determining Their Intrinsic Electrocatalytic Activity. Chem. Soc. Rev. 2019, 48 (9), 2518–2534.
- (21) Trotochaud, L.; Ranney, J. K.; Williams, K. N.; Boettcher, S. W. Solution-Cast Metal Oxide Thin Film Electrocatalysts for Oxygen Evolution. *J. Am. Chem. Soc.* **2012**, *134* (41), 17253–17261.
- (22) Kroschel, M.; Bonakdarpour, A.; Kwan, J. T. H.; Strasser, P.; Wilkinson, D. P. Analysis of Oxygen Evolving Catalyst Coated Membranes with Different Current Collectors Using a New Modified Rotating Disk Electrode Technique. *Electrochim. Acta* **2019**, 317, 722–736.
- (23) Ehsan, M. A.; Khan, A.; Zafar, M. N.; Akber, U. A.; Hakeem, A. S.; Nazar, M. F. Aerosol-Assisted Chemical Vapor Deposition of Nickel Sulfide Nanowires for Electrochemical Water Oxidation. *Int. J. Hydrog. Energy* **2022**, *47* (100), 42001–42012.